Energy Engineering

Tech Science Press

https://doi.org/10.32604/ee.2026.077403

ARTICLE

Coordinated Fault Ride-Through Strategy for Multi-Terminal VSC-HVDC System with Far-Offshore Wind Farms Integration

Qian Wu[1], Yang Wang[1], Yuchao Zheng[1], Linyuan Wang[1], Zhichao Yang[2] and Bingtuan Gao[2,*]

[1]State Grid Jiangsu Electric Power Co., Ltd. Economic and Technical Research Institute, Nanjing, China
[2]School of Electrical Engineering, Southeast University, Nanjing, China

*Corresponding Author: Bingtuan Gao. Email: gaobingtuan@seu.edu.cn

Received: 08 December 2025; Accepted: 02 February 2026; Published: 12 November 2026

ABSTRACT: With offshore wind power evolving toward clusterization in far-offshore areas, voltage source converter-based high voltage direct current (VSC-HVDC) technology remains the dominant transmission solution for connecting large-scale far-offshore wind farms to the onshore grid. To mitigate the DC overvoltage risk caused by active power imbalance in VSC-HVDC system integrated with far-offshore wind farms during onshore fault, a coordinated fault ride-through strategy is proposed in this paper. Firstly, the topology and mathematical model of a multi-terminal VSC-HVDC with permanent magnet synchronous generator-based offshore wind turbines (PMSG-OWTs) are established, and its transient behavior under fault condition is analyzed. Secondly, according to the fault voltage magnitude, pre-fault active power of VSC stations, and the number of faulty converter stations, the unbalanced power between sending-end VSC stations and receiving-end VSC stations is quantified. This quantified value is then used in conjunction with the voltage reduction region model to generate appropriate voltage reduction commands for the sending-end VSC stations. By adopting a common-outer-loop voltage reduction control scheme, the sending-end stations collectively and rapidly reduce their output power, thereby eliminating the power imbalance without resorting to additional hardware such as VSC choppers. Finally, simulation results demonstrate that the proposed strategy effectively reduces surplus power and suppresses DC overvoltage under onshore fault scenarios, significantly improving the transient resilience of multi-terminal VSC-HVDC system integrated with far-offshore wind farms.

KEYWORDS: Far-offshore wind farm; VSC-HVDC; onshore fault; voltage reduction region; fault ride-through

1 Introduction

As the global energy landscape shifts toward cleaner and low-carbon solutions [1], offshore wind farms have become a pivotal element in the development of wind power, owing to their abundant resources and high efficiency in power generation [2–4]. However, as offshore wind farms are positioned further from the coast, high voltage alternating current (HVAC) transmission technology faces limitations due to the capacitive charging current of submarine cables [5]. This necessitates the implementation of offshore compensation stations to extend the transmission range, making HVAC unsuitable for far-offshore applications. While low-frequency AC technology can be utilized for long-distance transmission, it is hindered by high costs and a lack of sufficient engineering experience [6]. In contrast, voltage source converter-based high voltage direct current (VSC-HVDC) technology offers the advantages of decoupled active and reactive power control, ease of connection to weak grids, and no inherent transmission distance limitations [7]. As such, it has emerged as an effective solution for integrating large-scale and long-distance offshore wind power [8,9].

Copyright © 2027 The Authors. Published by Tech Science Press. This work is licensed under a Creative Commons Attribution 4.0 International License, which permits unrestricted use, distribution, and reproduction in any medium, provided the original work is properly cited.

The interconnection of far-offshore wind farms with onshore systems relies on VSC-HVDC systems, which exhibit complex topologies and require extensive AC corridors [10]. In this context, reference [11] introduced a cost-effective, circuit breaker-less HVDC scheme that allows for the direct delivery of wind power to onshore systems via DC cables and overhead lines. Nevertheless, the extensive deployment of power electronic devices with limited individual capacity, coupled with the rapid dynamic response of VSC-HVDC system, amplifies overvoltage and overcurrent issues during fault conditions [12]. When an AC fault occurs at the receiving-end system, the power transfer capability of the receiving-end VSC station diminishes. If the sending-end wind farm does not correspondingly reduce its output power, excess power will continue to charge the DC-side capacitors, potentially causing DC overvoltage that could damage equipment and trigger VSC blocking [13].

Currently, two main approaches are employed to address these challenges. The first method aims to reduce the surplus power by curtailing the power of the sending-end wind farm. VSC stations can rapidly shed load through voltage reduction [14–16] or frequency raising methods [17,18], thereby lowering the active power injected by the sending-end VSC stations. Theoretically, these methods require no additional hardware. However, the complex active power response and weak primary frequency regulation capability of offshore wind farms may lead to slow response and limited control margin [19], casting uncertainty on the effectiveness of such strategies. To mitigate DC overvoltage caused by receiving-end fault, reference [15] proposed a two-stage voltage reduction scheme combined with voltage self-adaptive recovery for the entire fault ride-through process, employing a voltage-following active current control for current limitation. Although voltage reduction method responds faster than frequency raising method, an overly rapid voltage drop may cause overcurrent in the wind farm, while excessive reduction could trigger wind farm tripping [20]. Existing research on voltage reduction-based method overlooks the constraints imposed by the fault ride-through curve on the voltage command and duration, neglecting the practical voltage reduction region available to the offshore wind farm.

The second method involves the installation of chopper circuits to dissipate surplus power [21,22]. Current research primarily focuses on chopper topology, control, and placement. While chopper technology is well-established, offering fast response times and robust performance [23], the necessary rated capacity of the VSC chopper results in significant investment and maintenance costs [24]. To achieve a balance between reliability and cost, coordinated control schemes between the VSC-HVDC system and the chopper have been proposed to reduce the required capacity of the chopper circuit [25,26]. In [26], the VSC station can dynamically switch among conventional active power control, dynamic reactive current control, and chopper activation mode based on the fault depth, thereby maintaining active power balance and supporting voltage at the point of common coupling (PCC).

Conventional fault ride-through methods primarily focus on two-terminal VSC-HVDC systems and have several shortcomings. These include a lack of accurate surplus power calculation between sending-end and receiving-end VSC stations, which can lead to DC overvoltage. Additionally, these methods often overlook the voltage tolerance characteristics of far-offshore wind farms, and an inaccurate voltage reduction command may result in the tripping-off of offshore wind turbines. In systems with multiple VSC stations that employ independent outer-loop control, poor synchronization can occur, leading to sluggish power adjustments. When using the voltage reduction method for a more cost-effective fault ride-through, it becomes crucial to select the voltage reduction command rapidly and accurately. To address these limitations, this paper proposes a coordinated fault ride-through strategy aimed at enhancing the stability of multi-terminal VSC-HVDC system during onshore fault. The main contributions are as follows:

(1) A multi-terminal HVDC integration scheme for large-scale, far-offshore wind power is designed, taking into account key transient characteristics during onshore fault.

(2) The calculation model is established to address the unbalanced power between the sending-end and receiving-end VSC stations. This model factors in the pre-fault active power level, fault voltage depth, and the number of faulty VSC stations.

(3) The coordinated fault ride-through strategy based on the voltage reduction region and a common outer-loop controller is proposed. The proposed strategy effectively suppresses DC overvoltage in the multi-terminal VSC-HVDC system without the need for additional VSC chopper.

The structure of the remaining sections is organized as follows: Section 2 formulates the system model and analyzes the fault characteristics of multi-terminal HVDC integrated with far-offshore wind farms. Section 3 presents the proposed fault ride-through strategy. Simulation results are provided in Section 4, and conclusions are drawn in Section 5.

2 Multi-Terminal VSC-HVDC System

2.1 System Topology

Fig. 1 illustrates the topology of a multi-terminal VSC-HVDC system for integrating far-offshore wind farms. Far-offshore wind farms serve as an active power source, which comprises numerous permanent magnet synchronous generator-based offshore wind turbines (PMSG-OWTs). The VSC-HVDC system includes submarine cables and DC overhead lines, facilitated by three or more sending-end VSC stations that rectify the AC voltage of offshore wind turbine into the DC voltage. This setup enables long-distance power transmission from far-offshore sites to the onshore grid. Key protection devices equipped with high-speed switches and DC circuit breakers are also incorporated. In the onshore system, three or more receiving-end VSC stations invert the DC voltage to AC voltage. The proposed coordinated fault ride-through system acts as the central control unit, acquiring real-time data from all VSC stations via high-speed optical fiber channels to perform fault detection, power calculation, and command dispatch.

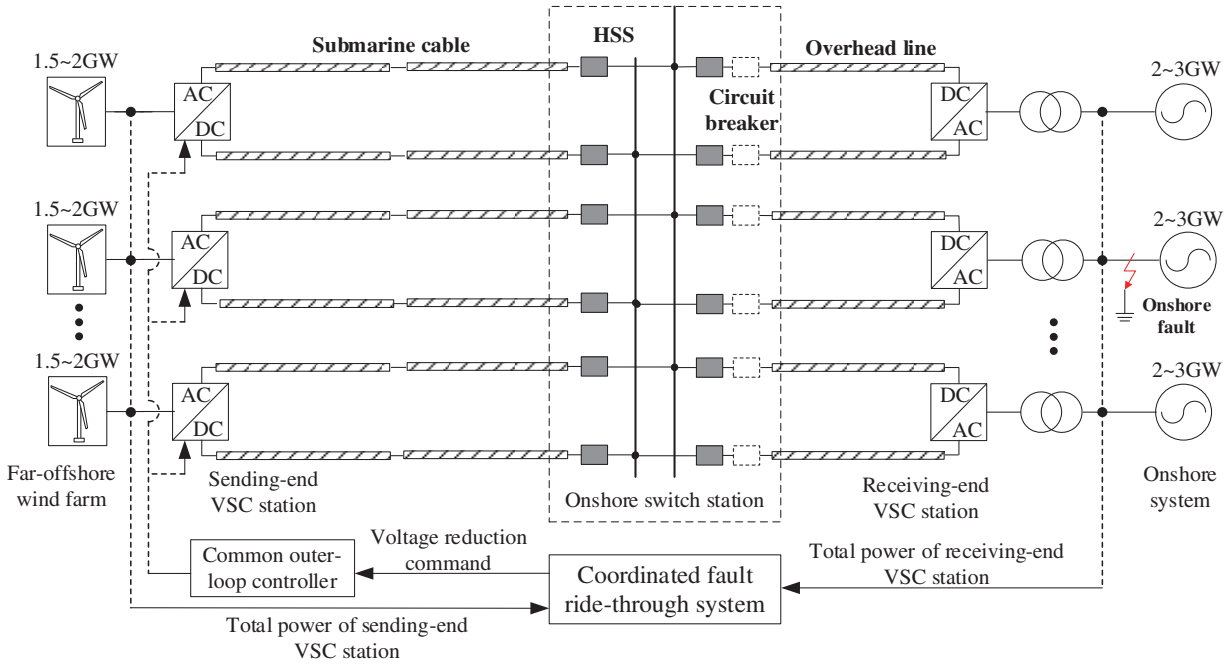


Figure 1: Topology of multi-terminal VSC-HVDC integrated far-offshore wind farms.

2.2 Mathematical Model and Control Strategies

PMSG-based offshore wind turbines are crucial part of far-offshore wind farm, which consist of PMSG, machine-side converter (MSC), grid-side converter (GSC) and OWT chopper. As depicted in Fig. 2, OWTs adopt MPPT controllers for the MSC and constant DC voltage controllers for GSC during stable operation.

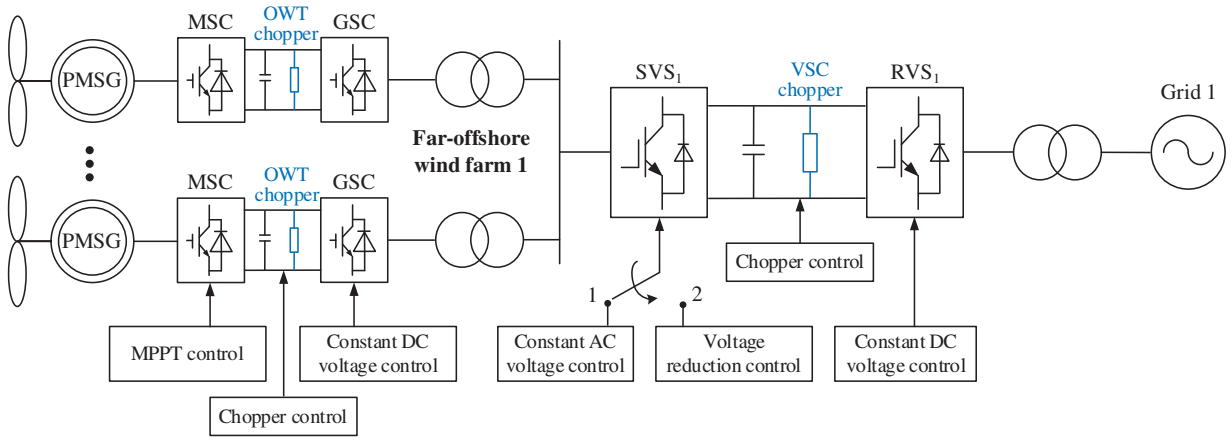


Figure 2: Simplified control system framework.

The mechanical power of offshore wind turbine can be calculated by [27]:

$$P_{\mathrm{m}} = \frac{1}{2}\rho\pi R^2 V^3 C_{\mathrm{p}} \tag{1}$$

where P_{m} is the mechanical power of OWT. ρ is the air density. R denotes the radius of OWT. V represents the wind speed, and C_{p} is the power coefficient.

OWT is configured with grid-following control strategy, where the current limit of GSC is set as 1.1 p.u. The grid-side voltage vector is oriented along the d-axis, and the output power given by GSC is [28]:

$$\begin{cases} P_{\mathrm{gsc}} = \dfrac{3}{2} U_{\mathrm{w}} I_{\mathrm{dw}} \\ Q_{\mathrm{gsc}} = -\dfrac{3}{2} U_{\mathrm{w}} I_{\mathrm{qw}} \end{cases} \tag{2}$$

where P_{gsc} and Q_{gsc} are the active power and reactive power of the OWT, respectively. U_{w} is the AC voltage of OWT. I_{dw} and I_{qw} are the active current and reactive current, respectively.

Assuming no power loss, the DC-link voltage of the OWT is described as:

$$C_{\mathrm{w}} U_{\mathrm{dcw}} \frac{\mathrm{d}U_{\mathrm{dcw}}}{\mathrm{d}t} = P_{\mathrm{rsc}} - P_{\mathrm{gsc}} = P_{\mathrm{m}} - P_{\mathrm{gsc}} \tag{3}$$

where C_{w} is the equivalent DC capacitance of the OWT. U_{dcw} denotes the DC link voltage of the OWT. P_{rsc} is the active power of RSC.

OWTs transmit wind power to the onshore system via VSC-HVDC, and the active power of the sending-end VSC station (SVS) is:

$$P_{\mathrm{sf}} = P_{\mathrm{w}} = \sum_{i=1}^{n_1} P_{\mathrm{w}i} \tag{4}$$

where P_{sf} is the active power of SVS. P_w is the total active power of a far-offshore wind farm. n_1 is the number of OWTs, and P_{wi} is the active power of OWT i.

Taking into account the power balance of the sending-end and receiving-end VSC stations. If VSC chopper is not activated, the dynamic equation of DC capacitor of VSC-HVDC is:

$$C_{hvdc}U_{hvdc}\frac{dU_{hvdc}}{dt} = P_{sf} - P_{rf} \tag{5}$$

where C_{hvdc} is the equivalent DC capacitance of VSC-HVDC. U_{hvdc} represents the DC link voltage of VSC-HVDC, and P_{rf} is the active power of the receiving-end VSC station (RVS).

2.3 Fault Characteristics

When an AC fault occurs in the onshore receiving-end system, the voltage of the receiving-end VSC station drops sharply, triggering the DC overvoltage of VSC-HVDC system. At this point, the sending-end VSC station switches from control mode 1 to control mode 2, as shown in Fig. 2. When further considering the chopper circuit, the power flow of multi-terminal VSC-HVDC integrated with far-offshore wind farms is depicted in Fig. 3.

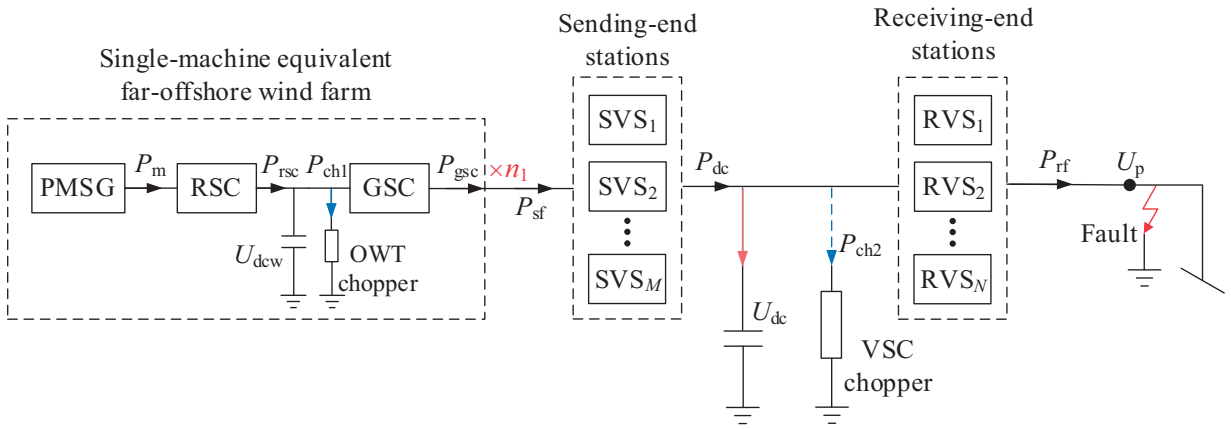


Figure 3: Power flow of multi-terminal VSC-HVDC.

Due to the voltage drop, the active current output of the faulty VSC station is constrained by the maximum current (I_{mr}) of the VSC station and the transient reactive current, resulting in a sudden drop in the total active power (P_{rf}). Due to the physical isolation of the HVDC system, the sending-end VSC station cannot directly detect the fault voltage at the receiving-end system. The total active power (P_{sf}) of the sending-end VSC station remains at the pre-fault level in the short term, leading to $P_{sf} > P_{rf}$. According to Eq. (5), the power difference ΔP accumulates in VSC-HVDC can cause DC overvoltage.

The single-machine equivalent method is applied to represent the far-offshore wind farm. Substituting Eq. (4) into Eq. (5), it can be obtained that:

$$\Delta P = C_{hvdc}U_{hvdc}\frac{dU_{hvdc}}{dt} = \sum_{i=1}^{n_1} P_{wi} - P_{rf} = n_1 P_m - P_{rf} \tag{6}$$

Further considering the function of chopper circuit, the DC voltage of VSC-HVDC can be calculated according to:

$$\Delta P = C_{\text{hvdc}} U_{\text{hvdc}} \frac{\mathrm{d}U_{\text{hvdc}}}{\mathrm{d}t} = n_1 \left(P_m - P_{\text{ch1}}\right) - \left(P_{\text{rf}} + P_{\text{ch2}}\right) \tag{7}$$

where, P_{ch1} and P_{ch2} is the absorbed power of OWT chopper and VSC chopper.

According to Eq. (7), the utilization of chopper during onshore fault can reduce the power difference of HVDC system, thereby reducing the risk of DC overvoltage. The response processes of DC overvoltage under different strategies are shown in Fig. 4. If the fault ride through strategy is not adopted during onshore grid fault, the DC voltage of VSC-HVDC may exceed the upper limit (U_{dm}), thereby triggering DC protection actions. When using chopper, the surplus power between the sending-end and receiving-end VSC stations can be absorbed by VSC chopper or OWT chopper, thereby suppressing the rise of DC voltage to a certain extent. Considering the voltage drop method and the overcurrent capability of sending-end VSC station, the degree of DC overvoltage can be further reduced, improving the fault ride through capability of the multi-terminal VSC-HVDC system.

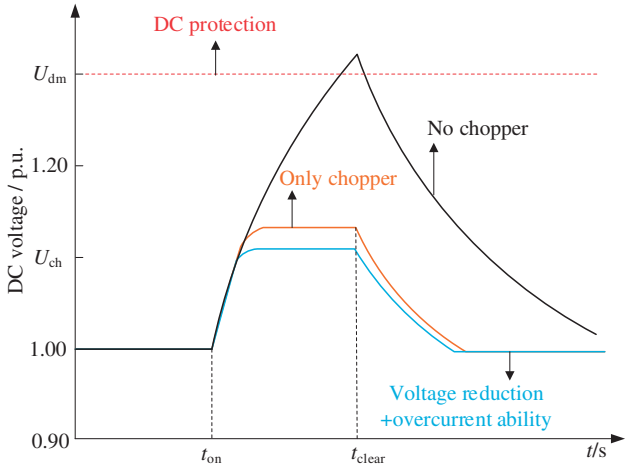


Figure 4: DC voltage response of VSC-HVDC.

When the sending-end VSC station adopts the voltage reduction method, OWT may enter the low voltage ride through mode. When the DC voltage is higher than 1.08 p.u., the OWT chopper is triggered, and the DC voltage trajectory is basically the same as that of VSC-HVDC. Considering the high investment of VSC chopper, this paper intends to use OWT chopper to absorb transient surplus power, ensuring that the DC voltage of both OWT and VSC-HVDC are suppressed during onshore fault.

3 Proposed Strategy

3.1 Total Active Power of Receiving-End Stations

The coordinated fault ride-through control system acquires key data of receiving-end VSC stations via high-speed optical fiber channels, including fault voltage of faulty station i ($U_{\text{pf}i}$), AC voltage of non-faulty station j ($U_{\text{ps}j}$), the pre-fault active current ($I_{\text{dr}i}$), number of faulty converter stations (N_1), and number of non-faulty converter stations (N_2). Based on the above information, the total active power of receiving-end VSC stations (P_{rf}) can be calculated.

After the receiving-end VSC station i enters the fault ride-through mode, its active current $I_{\mathrm{dr}i}$ is limited by both the pre-fault power and the overload capacity of VSC station, which can be described by the following piecewise function:

$$I_{\mathrm{dr}i} = \begin{cases} I_{\mathrm{d0}i}, 0.9 \le U_{\mathrm{pf}} \le 1 \\ \min\left(I_{\mathrm{d0}i}, \sqrt{I_{\mathrm{mr}}^2 - \left(k_{\mathrm{f}} \cdot \left(0.9 - U_{\mathrm{pf}i}\right)\right)^2}\right), 0 \le U_{\mathrm{pf}} < 0.9 \end{cases} \tag{8}$$

where, $I_{\mathrm{d0}i}$ is the active current of VSC station i before the fault. I_{mr} is the maximum allowable current of the receiving-end VSC station, and k_{f} is the transient reactive current coefficient. $U_{\mathrm{pf}i}$ is the AC voltage of faulty station i.

The total active power of N receiving-end VSC stations ($N = N_1 + N_2$) during the fault is the sum of the power of faulty and non-faulty VSC stations, the total active power of receiving-end VSC stations is:

$$P_{\mathrm{rf}} = \sum_{i=1}^{N_1} \left(U_{\mathrm{pf}i} \cdot I_{\mathrm{dr}i}\right) + \sum_{j=1}^{N_2} \left(U_{\mathrm{ps}j} \cdot I_{\mathrm{ds}j}\right) \tag{9}$$

where, $U_{\mathrm{pf}i}$ is the AC voltage of non-faulty station i. $I_{\mathrm{ds}j}$ is the active current of non-faulty station j.

3.2 Deloading Power of Sending-End Stations

The total active power of all sending-end VSC stations is:

$$P_{\mathrm{sf}} = \sum_{m=1}^{M} \left(U_{\mathrm{s}} \cdot I_{\mathrm{ds}m}\right) \tag{10}$$

where, M is the number of sending-end VSC stations, P_{sf} is the total active power of the sending-end VSC stations, U_{s} is the voltage of the sending-end system, and $I_{\mathrm{ds}m}$ is the aggregated active current of sending-end VSC station m.

Substituting Eq. (9) into Eq. (10), the total active power difference between the sending-end and receiving-end VSC stations is:

$$\Delta P = P_{\mathrm{sf}} - P_{\mathrm{rf}} = \sum_{m=1}^{M} \left(U_{\mathrm{s}} \cdot I_{\mathrm{ds}m}\right) - \sum_{i=1}^{N_1} \left(U_{\mathrm{pf}i} \cdot I_{\mathrm{dr}i}\right) - \sum_{j=1}^{N_2} \left(U_{\mathrm{ps}j} \cdot I_{\mathrm{ds}j}\right) \tag{11}$$

where, ΔP is the comprehensive reduction power that needs to be cut by the sending-end VSC stations.

To prevent far-offshore wind turbines from trip-off due to voltage reduction on the sending-end system, a voltage-time dimensional voltage reduction region is established, as illustrated in Fig. 5, to define the allowable range for the voltage reduction command.

VSC station and far-offshore wind turbines have zero-voltage ride-through capability, allowing an operating voltage range of [0 p.u., 1 p.u.], which can be divided into 4 stages according to [29,30]. The fault ride-through requirements for offshore wind turbines specified in the grid codes are equally applicable to VSC-HVDC systems. For the purpose of uninterrupted operation of VSC station and far-offshore wind turbines, the duration should satisfy:

$$t_{\mathrm{r}} = \begin{cases} 0.25, 0 \le U_{\mathrm{sf}} < 0.2 \\ 0.625, U_{\mathrm{sf}} = 0.2 \\ 1.964 U_{\mathrm{sf}} + 0.232, 0.2 \le U_{\mathrm{sf}} \le 0.9 \\ \infty, 0.9 < U_{\mathrm{sf}} \le 1 \end{cases} \tag{12}$$

where t_r is the continuous low-voltage operation time of far-offshore wind turbines, and U_{sf} is the voltage reduction command of the sending-end VSC station.

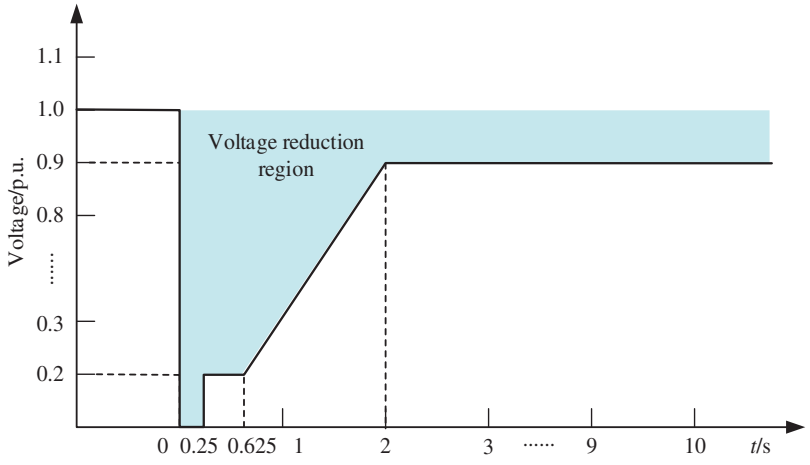


Figure 5: Voltage reduction region of VSC station.

When the voltage reduction command U_{sf} is in [0, 0.2 p.u.), the maximum continuous operation time of far-offshore wind turbines is 0.25 s. If the voltage reduction command is 0.2 p.u., the maximum continuous operation time of far-offshore wind turbines is 0.625 s. While the voltage reduction command is in [0.2, 0.9 p.u.], the maximum continuous operation time of far-offshore wind turbines is calculated according to Eq. (12). When the step-down operation command U_{sf} is in (0.9, 1 p.u.], the continuous operation time of offshore wind turbines is not limited.

To eliminate the surplus power between sending-end and receiving-end VSC stations during onshore fault, Eq. (11) should be set to zero. Accordingly, the voltage command for the sending-end VSC station is adjusted as follows:

$$U_{sf} = \frac{\sum_{i=1}^{N_1} \left(U_{pf} \cdot I_{dri}\right) + \sum_{j=1}^{N_2} \left(U_{ps} \cdot I_{dsj}\right)}{\sum_{m=1}^{M} I_{dsm}} \tag{13}$$

The voltage command must comply with the boundaries of the voltage reduction region (i.e., $U_{sf} \in [0\ \text{p.u.}, 1\ \text{p.u.}]$) and its operation time (t_r) must not exceed the tolerance limit of far-offshore wind turbines. If these conditions are not met, the voltage reduction command must be revised to prevent the far-offshore wind turbines from trip-off issue.

3.3 Coordinated Fault Ride-Through Strategy

The fault ride-through command is delivered through the outer-loop and inner-loop controllers of the VSC-HVDC system. In traditional multi-terminal configurations, the sending-end VSC station typically employs an independent outer-loop controller, as illustrated in Fig. 6. This decentralized control structure leads to deviations in the voltage references among VSC stations, resulting in poorly synchronized and delayed power adjustments.

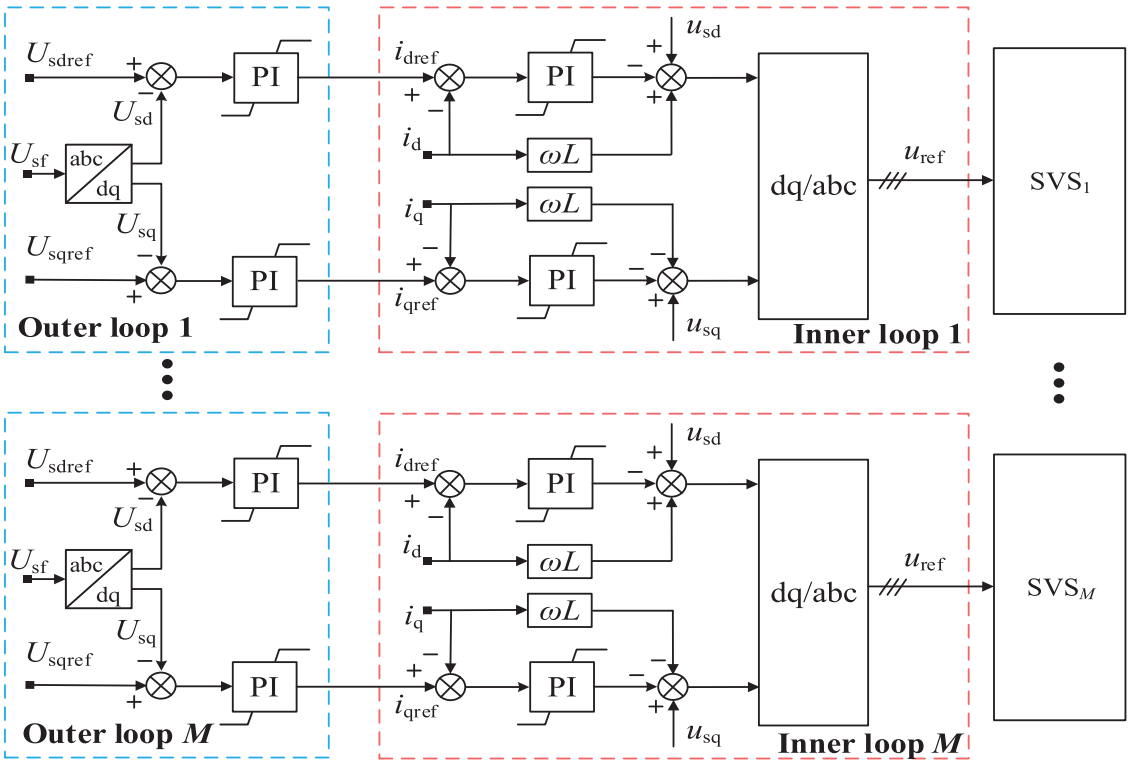


Figure 6: Traditional independent outer-loop control structure for VSC stations.

This paper proposes a common outer-loop voltage reduction control strategy, as illustrated in Fig. 7. Instead of employing independent outer-loop controllers for each sending-end VSC station, a single common outer-loop controller is used to generate unified voltage reduction commands and distribute them to all sending-end VSC stations. This architecture offers the advantages of a simplified control structure and reduced system complexity. Since all sending-end VSC stations operate with the same voltage reference, the potential superposition of voltage fluctuations is effectively avoided. As a result, the transmitted power from the sending-end VSC stations can be rapidly reduced, enabling the elimination of power imbalance in a short time. This approach facilitates coordinated fault ride-through by harmonizing the responses of the sending-end and receiving-end VSC stations.

The detailed control flowchart of the proposed strategy is shown in Fig. 8. The specific process includes: When the coordinated fault ride-through control system detects an AC fault in the onshore system, it calculates in real time the total active power of the receiving-end VSC stations based on the fault voltage at the point of common coupling, the pre-fault active power of VSC stations, and the number of faulty VSC stations. Based on the power difference between the total active power of the receiving-end VSC stations and the total active power of the sending-end VSC stations, it calculates the comprehensive reduction power of the sending-end VSC stations, and further generates the voltage reduction command for the sending-end VSC stations through the embedded voltage reduction region model of VSC stations. The sending-end VSC stations adopt common outer-loop voltage reduction control to actively reduce the AC voltage of the sending-end system, causing the active power of far-offshore wind farms to drop rapidly, eliminating the active power difference between the sending-end and receiving-end VSC stations, thus realizing the coordinated AC fault ride-through control of VSC-HVDC. This invention can reduce the power redundancy and DC overvoltage risk of the multi-terminal VSC-HVDC system during fault, improving the system's fault resistance capability.

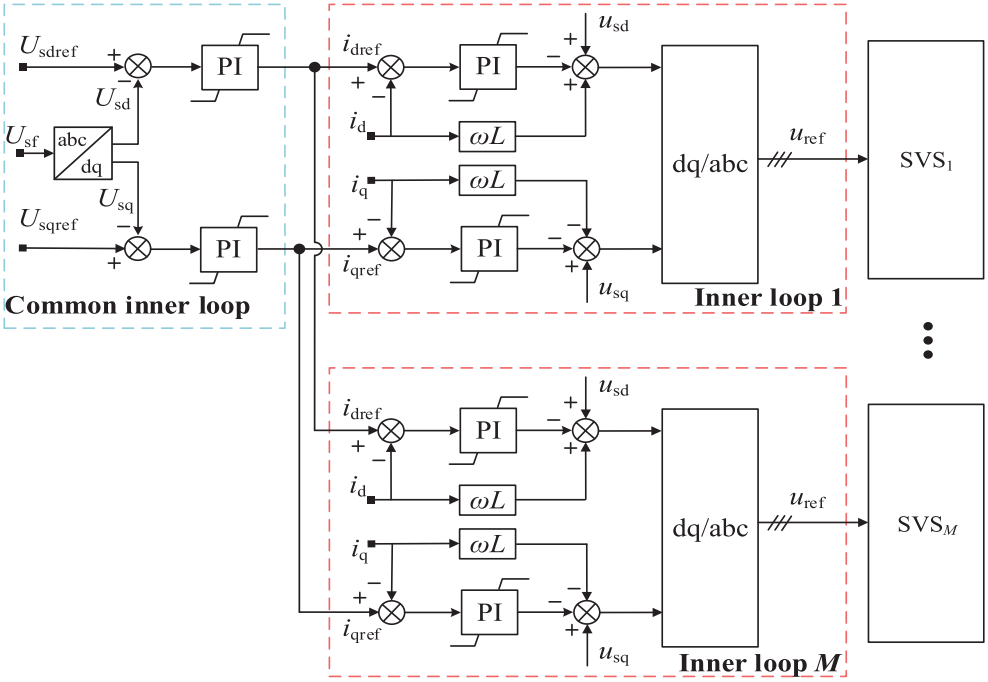


Figure 7: Common outer-loop voltage reduction control for VSC stations.

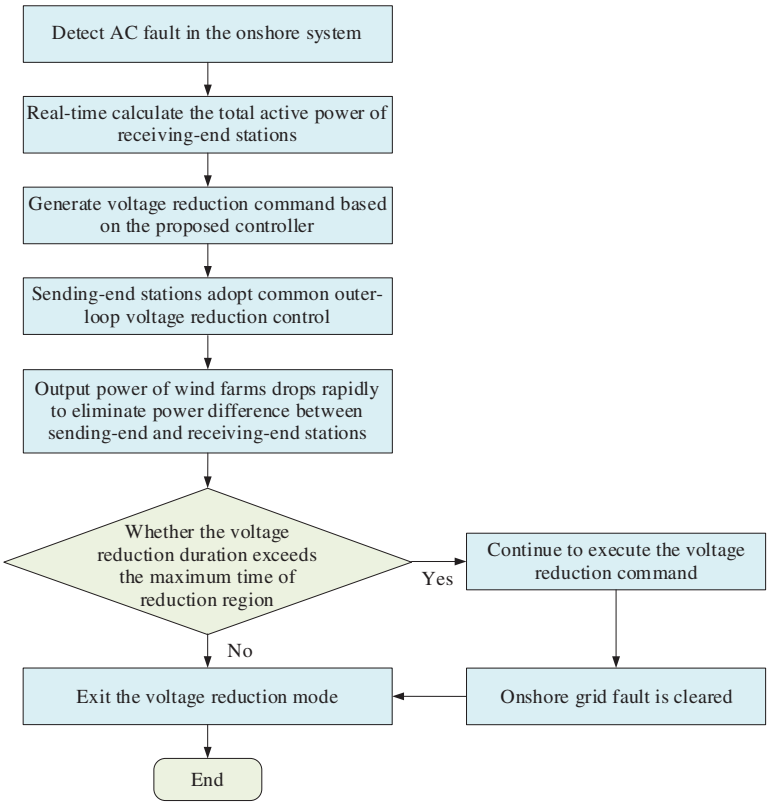


Figure 8: Detailed flowchart of the proposed strategy.

4 Case Study

4.1 System Settings

To verify the effectiveness of the proposed fault ride-through strategy, simulation verification is conducted in PSCAD software. The test system consists of six-terminal VSC-HVDC and far-offshore wind farms, of which the rated capacity is 6 GW. The sending-end system contains three far-offshore wind farms, which are linked to SVS_1 (1600 MW), SVS_2 (1600 MW) and SVS_3 (1600 MW), respectively. The receiving-end system contains RVS_1 (1600 MW), RVS_2 (1600 MW), and RVS_3 (1600 MW). The VSC-HVDC system adopts a pseudo-bipolar structure with a rated voltage of ±500 kV, and the AC voltage of the receiving-end system is 380 kV. The far-offshore wind farms consist of PMSG-based wind turbines. When focusing on the external characteristics of the far-offshore wind farms, the equivalent method can be used to equate the far-offshore wind farm to a single-machine aggregated model, thereby reducing the difficulty of system modeling and simulation time. The system structure is depicted in Fig. 9, and the specific parameters are listed in Table 1.

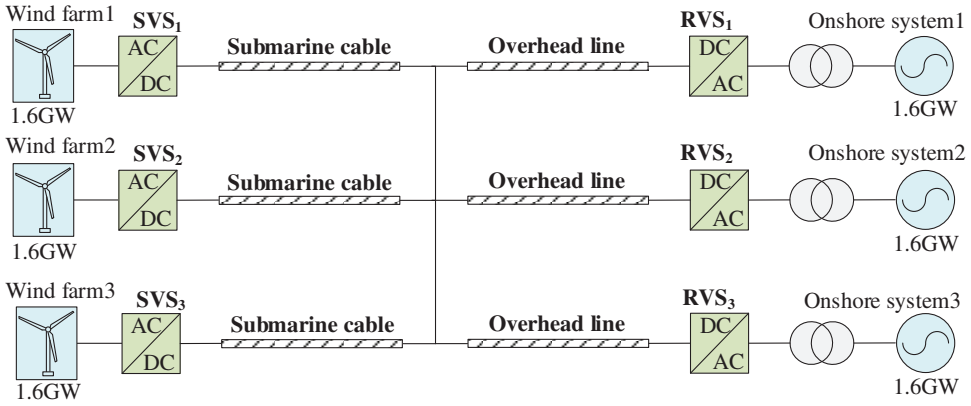


Figure 9: Topology of six-terminal VSC-HVDC with far-offshore wind farms.

Table 1: Basic parameters of test system.

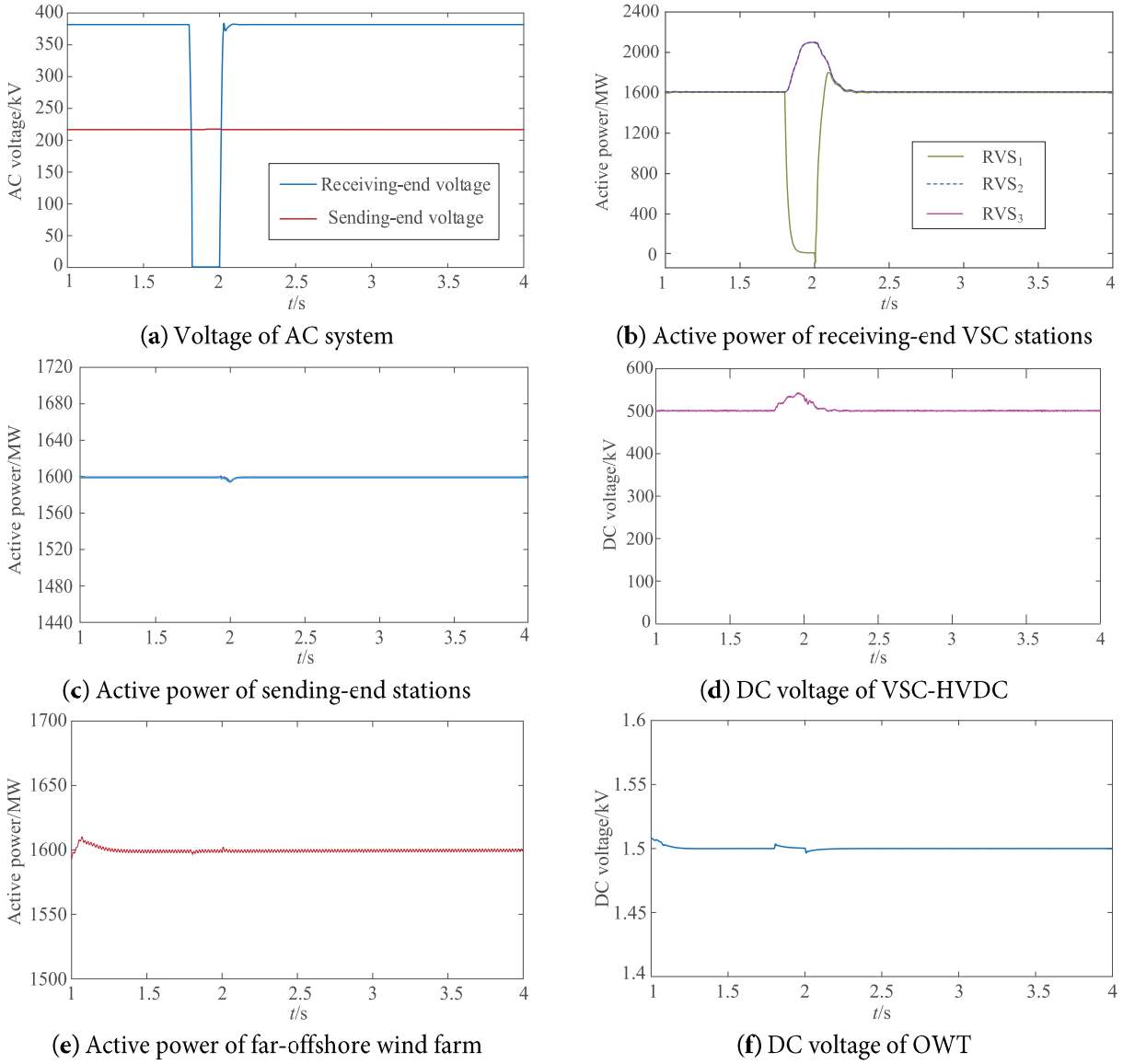
VSC-HVDC	Sending-End System	Receiving-End System
Rate power/MW	4800	4800
VSC stations	SVS_1~SVS_3	RVS_1~RVS_3
DC voltage/kV	±500	±500
AC voltage/kV	220	380
Capacity of transformer/MVA	1650	1650
Ratio of transformer/kV	220/525	525/500
Length of submarine cables	120 km	
Length of overhead lines	200 km	
Frequency of AC system/Hz	50	

4.2 Simulation Results

(1) Case 1: A three-phase short-circuit fault is configured in onshore system 1 interconnected with RVS_1. Specifically, the fault occurs at 1.8 s with a duration of 0.2 s and a fault depth of 1 p.u. The total active power of far-offshore wind farms is 4800 MW. For comparison, the traditional strategy utilizing the

overload capacity of non-faulty VSC stations and VSC choppers is evaluated against the proposed strategy, with the corresponding results presented in Figs. 10 and 11.

Fig. 10a depicts the AC voltage waveform during the occurrence of a fault in the onshore system 1. When the AC voltage drops to zero, the active power of RVS_1 decreases to zero correspondingly, as illustrated in Fig. 10b. Under the traditional control strategy, RVS_2 and RVS_3 maintain their rated power of 1600 MW. As shown in Fig. 10c, the active power of the sending-end VSC stations remains essentially unchanged, which consequently causes the DC voltage to rise from 500 kV to 544 kV according to Fig. 10d. Fig. 10e indicates that since the voltage of the sending-end VSC station stays constant, the active power of the far-offshore wind farm does not respond to the onshore fault voltage and remains stable at 1600 MW throughout the fault period. Fig. 10f shows that the DC voltage of the offshore wind turbines remains largely stable without significant fluctuations.



(**a**) Voltage of AC system

(**b**) Active power of receiving-end VSC stations

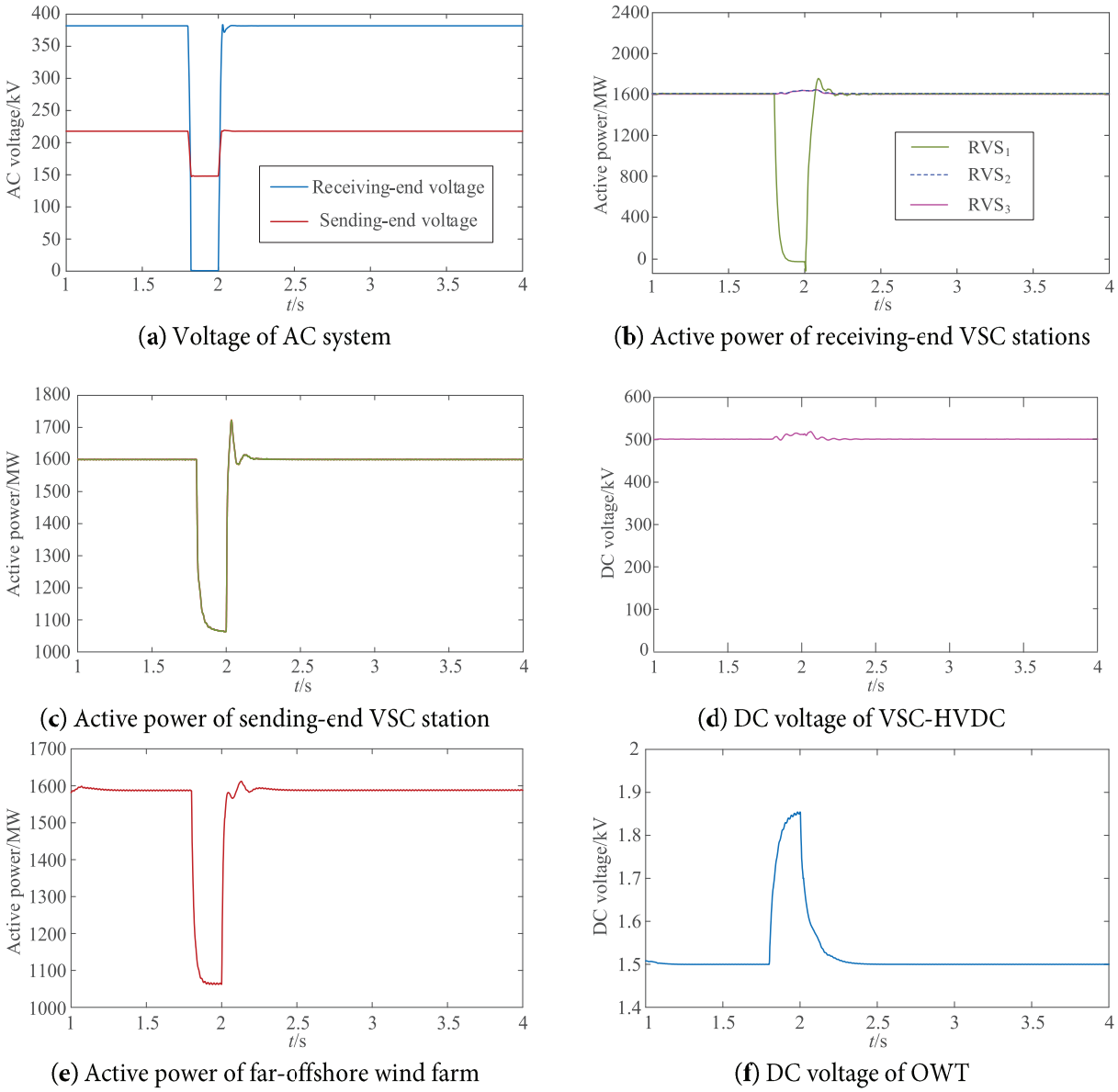
(**c**) Active power of sending-end stations

(**d**) DC voltage of VSC-HVDC

(**e**) Active power of far-offshore wind farm

(**f**) DC voltage of OWT

Figure 10: System response under the traditional strategy.



(**a**) Voltage of AC system

(**b**) Active power of receiving-end VSC stations

(**c**) Active power of sending-end VSC station

(**d**) DC voltage of VSC-HVDC

(**e**) Active power of far-offshore wind farm

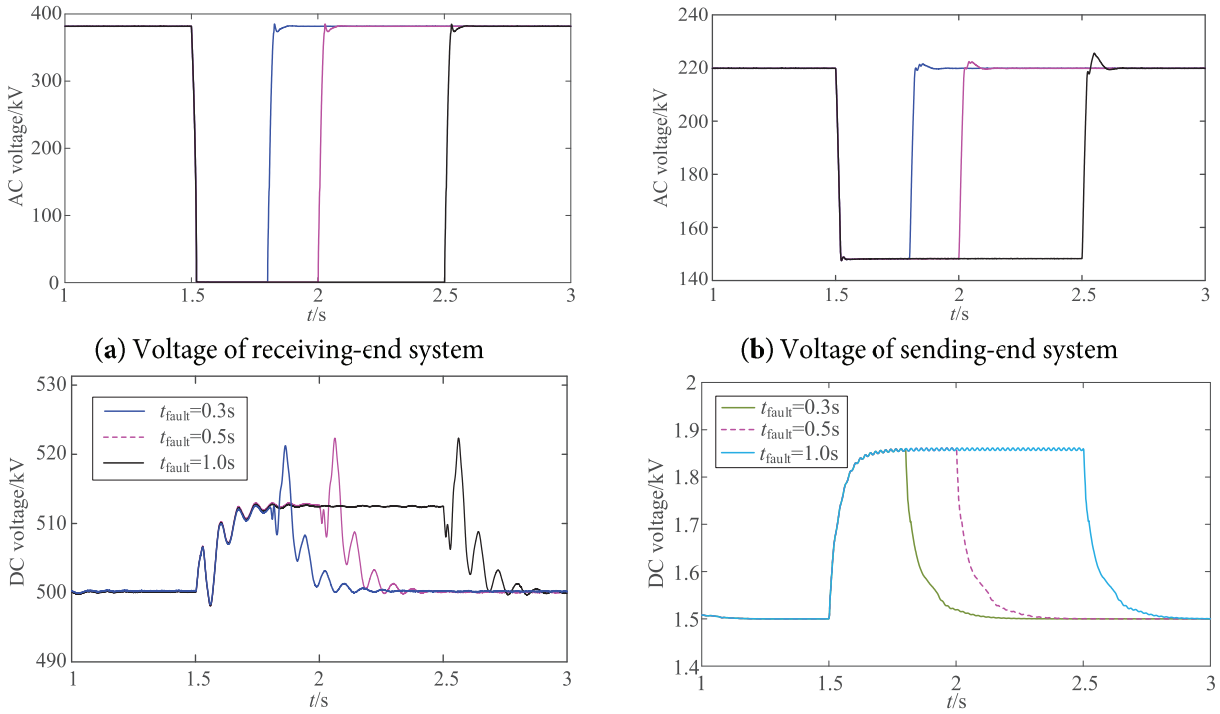
(**f**) DC voltage of OWT

Figure 11: System response under the proposed strategy.

When the multi-terminal VSC-HVDC system adopts the proposed strategy, the sending-end VSC stations can regulate the AC voltage of the sending-end system according to the power drop degree of the receiving-end VSC stations, reducing the sending-end AC voltage to 146.7 kV in Fig. 11a. Following a voltage dip in onshore system 1, the active power of RVS_1 drops to 0. In contrast, as illustrated in Fig. 11b, the active power of RVS2 and RVS3 remains stable at 1600 MW. As presented in Fig. 11c, the active power of SVS_1~SVS_3 all decrease from 1600 to 1067 MW, thereby essentially eliminating the unbalanced power between the sending-end and receiving-end systems. Thus, the DC voltage only increases moderately from 500 to 512 kV as shown in Fig. 11d. Under the critical scenario where the voltage drops to zero, compared to the traditional strategy, the proposed strategy can reduce the DC voltage of VSC-HVDC from 544 to 512 kV, representing a decrease of 6.25%. Fig. 11e demonstrates that the active power of far-offshore wind farm declines with the voltage drop in the sending-end VSC station, falling from the initial 1600 to 1070 MW at 1.85 s. According

to Fig. 11f, since the offshore wind turbines enter low voltage ride-through mode, the DC voltage rises to 1.85 kV (1.23 p.u.), which is within the allowable threshold of 1.3 p.u. Therefore, the proposed strategy can effectively enhance the fault ride-through capability of far-offshore wind farms integrated via multi-terminal VSC-HVDC system, and mitigate the DC overvoltage risk during onshore fault without additional hardware costs.

(2) Case 2: To investigate the impact of fault duration on the proposed strategy, a three-phase fault occurs in onshore system 2 interconnected with RVS_2, with fault duration set to 0.3, 0.5, and 1.0 s, respectively. The corresponding simulation results are presented in Fig. 12.



(**a**) Voltage of receiving-end system

(**b**) Voltage of sending-end system

(**c**) DC voltage of VSC-HVDC

(**d**) DC voltage of OWT

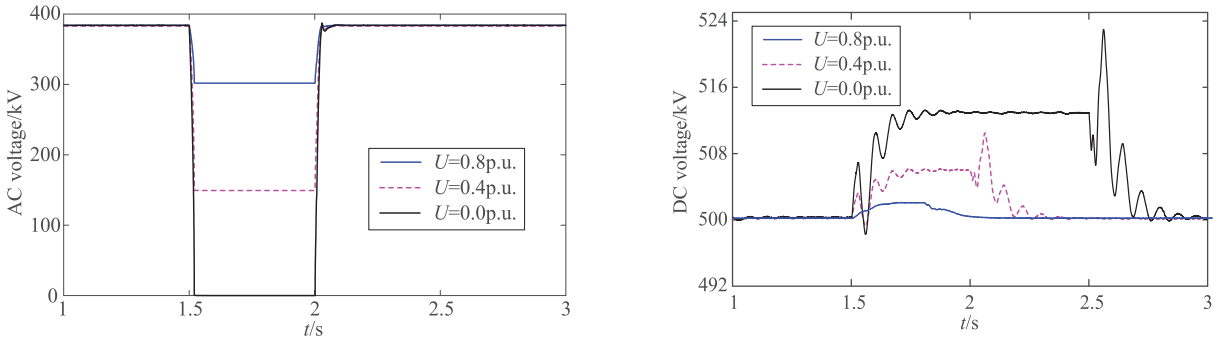
Figure 12: DC voltage under different fault duration conditions.

As illustrated in Fig. 12a, when the fault duration varies, the AC voltage of receiving-end system 2 drops to zero. Fig. 12b indicates that the magnitude of the voltage drop in the sending-end system remains consistent, while the voltage reduction operation and fault recovery time differ under different fault duration conditions. As shown in Fig. 12c, the DC voltage rises to 512.1 kV in all three scenarios, without exceeding the voltage limit of 650 kV. Fig. 12d indicates that under different fault duration conditions, the DC voltage of OWT increases from 1.5 kV to a peak value of 1.85 kV. During the onshore fault, the active power of the offshore wind farm decreases, but no tripping-off issue occurs due to DC overvoltage. Therefore, the fault duration has little impact on the magnitude of DC overvoltage. However, a longer fault duration results in an extended DC voltage recovery time of the multi-terminal VSC-HVDC system.

(3) Case 3: To investigate the impact of different fault depths, the voltage of onshore system 1 is set to drop to 0, 0.4, and 0.8 p.u., respectively. The simulation results are shown in Fig. 13.

As depicted in Fig. 13, when the AC voltage of onshore system 1 drops to 0, 0.4, and 0.8 p.u., the DC voltage rises to 502.3, 506.7, and 512.2 kV, respectively. It can be concluded that a more significant

drop in onshore voltage leads to additional unbalanced power in the multi-terminal VSC-HVDC system, resulting in a more pronounced DC overvoltage issue. The proposed coordinated fault ride-through strategy can effectively handle different fault durations and voltage dip conditions, thereby enhancing the fault ride-through capability of multi-terminal VSC-HVDC system integrated with far-offshore wind farms.



(**a**) Voltage of receiving-end system (**b**) DC voltage of VSC-HVDC

Figure 13: DC voltage under different voltage dip conditions.

The above simulation results demonstrate that the proposed strategy eliminates the VSC chopper, significantly reducing the cost of fault ride-through while enhancing the fault ride-through capability of multi-terminal VSC-HVDC system integrated with far-offshore wind farms. In particular, when the AC voltage of onshore grid drops to zero, the proposed strategy can reduce the DC voltage of VSC-HVDC by 6.25% compared to the traditional strategy.

5 Conclusions

This paper proposes a coordinated fault ride-through strategy to enhance the transient stability of the multi-terminal VSC-HVDC system integrated with far-offshore wind farms during onshore fault. The key conclusions are as follows:

(1) A multi-terminal VSC-HVDC system, suitable for large-scale transmission of far-offshore wind power, is established. During onshore fault, unbalanced power between the sending-end and receiving-end VSC stations can lead to DC-side overvoltage.

(2) By utilizing information including the pre-fault active power level, fault voltage depth, and the number of faulty VSC stations, unbalanced power between the sending-end and receiving-end systems can be accurately calculated. Voltage reduction commands for the sending-end VSC stations are generated using the voltage reduction region model, which effectively reduces the active power of the sending-end system quickly.

(3) Simulation results verify that the proposed strategy enhances the fault ride-through capability of the multi-terminal VSC-HVDC system integrated with far-offshore wind farms by effectively suppressing DC overvoltage. The proposed strategy is readily applied to actual VSC-HVDC projects of various capacities by modifying the control system, thus avoiding the hardware costs associated with changes to VSC modules or chopper circuits.

Future research will focus on the impacts of wind resource variability and wind turbine heterogeneity on the fault ride-through control strategy. Additionally, further studies are needed on the transient control strategies that meet grid requirements, including reactive power support and DC overvoltage suppression.

Acknowledgement: None.

Funding Statement: This research was funded by the Technology Project of State Grid Jiangsu Electric Power Co., Ltd., Grant Number J2025026.

Author Contributions: The authors confirm their contributions to this article as follows: study conception and design: Qian Wu; data collection: Yang Wang; modelling: Yuchao Zheng, Linyuan Wang; analysis and interpretation of results: Zhichao Yang; draft manuscript preparation: Bingtuan Gao. All authors reviewed and approved the final version of the manuscript.

Availability of Data and Materials: The data that support the findings of this study are available from the corresponding author upon reasonable request.

Ethics Approval: Not applicable.

Conflicts of Interest: The authors declare no conflicts of interest.

References

1. Qian Z, Ma H, Rao J, Hu J, Yu L, Feng C, et al. Research on reactive power optimization of offshore wind farms based on improved particle swarm optimization. Energy Eng. 2023;120(9):2013–27. doi:10.32604/ee.2023.028859.
2. Su X, Wang X, Xu W, Yuan L, Xiong C, Chen J. Offshore wind power: progress of the edge tool, which can promote sustainable energy development. Sustainability. 2024;16(17):7810. doi:10.3390/su16177810.
3. Rowell D, McMillan D, Carroll J. Offshore wind H&S: a review and analysis. Renew Sustain Energy Rev. 2024;189:113928. doi:10.1016/j.rser.2023.113928.
4. Deng J, Cheng F, Yao L, Xu J, Mao B, Li X, et al. A review of system topologies, key operation and control technologies for offshore wind power transmission based on HVDC. IET Gener Transm Distrib. 2023;17(15):3345–63. doi:10.1049/gtd2.12894.
5. Lyu Y, Luo Y, Jia Z, Fu S, Tang Y, Wang Q, et al. Benefit evaluation of HVAC and HVDC for offshore wind power transmission system under the multidimensional index. Electr Power Syst Res. 2024;237:111018. doi:10.1016/j.epsr.2024.111018.
6. Yang B, Liu B, Zhou H, Wang J, Yao W, Wu S, et al. A critical survey of technologies of large offshore wind farm integration: summary, advances, and perspectives. Prot Control Mod Power Syst. 2022;7(1):17. doi:10.1186/s41601-022-00239-w.
7. Bimenyimana S, Wang C, Norense Osarumwense Asemota G, Nduwamungu A, Mulolani F, De Dieu Niyonteze J, et al. Fault ride-through (FRT) behavior in VSC-HVDC as key enabler of transmission systems using SCADA viewer software. Energy Eng. 2022;119(6):2369–406. doi:10.32604/ee.2022.019257.
8. Jiang S, Xin Y, Li G, Wang L. A novel DC fault ride-through method for wind farms connected to the grid through bipolar MMC-HVDC transmission. IEEE Trans Power Deliv. 2020;35(6):2937–50. doi:10.1109/TPWRD.2020.2991722.
9. Cao P, Fan H, Cai Z. Adaptive fractional-order PID control for VSC-HVDC systems via cooperative beetle antennae search with offshore wind integration. Energy Eng. 2021;118(2):265–84. doi:10.32604/ee.2021.014513.
10. Yu Z, Song Q, Yuan Z, Zou C, Qiao X, Liu W. Transmission topology and control for ultra-large offshore wind bases integrating multiple offshore low-frequency AC links and onshore HVDC link. IEEE Trans Power Deliv. 2024;39(5):2797–809. doi:10.1109/TPWRD.2024.3432897.
11. Liu X, Mei X, Xiang W, Li F, Peng S, Zou C, et al. DBS-less MMC-MTDC system integrating large-scale offshore wind power. Electr Power Syst Res. 2025;244:111589. doi:10.1016/j.epsr.2025.111589.
12. Shi L, Adam GP, Li R, Xu L. Control of offshore MMC during asymmetric offshore AC faults for wind power transmission. IEEE J Emerg Sel Top Power Electron. 2020;8(2):1074–83. doi:10.1109/JESTPE.2019.2930399.

13. Cao S, Xiang W, Lu X, Lin W, Zhang K, Wen J, et al. Energy dissipation of MMC-HVDC based onshore wind power integration system with FB-DBS and DCCB. IET Renew Power Gener. 2020;14(2):222–30. doi:10.1049/iet-rpg.2019.0491.
14. Erlich I, Feltes C, Shewarega F. Enhanced voltage drop control by VSC–HVDC systems for improving wind farm fault ridethrough capability. IEEE Trans Power Deliv. 2014;29(1):378–85. doi:10.1109/TPWRD.2013.2285236.
15. Li W, Zhu M, Chao P, Liang X, Xu D. Enhanced FRT and postfault recovery control for MMC-HVDC connected offshore wind farms. IEEE Trans Power Syst. 2020;35(2):1606–17. doi:10.1109/TPWRS.2019.2944940.
16. Zhu M, Li W, Liang X, Xu S, Zhou B, Shen Y. Stepwise voltage drop and transient current control strategies to enhance fault ride-through capability of MMC-HVDC connected DFIG wind farms. IEEE Trans Power Syst. 2021;36(3):2127–37. doi:10.1109/TPWRS.2020.3026082.
17. Hu X, Liang J, Rogers DJ, Li Y. Power flow and power reduction control using variable frequency of offshore AC grids. IEEE Trans Power Syst. 2013;28(4):3897–905. doi:10.1109/TPWRS.2013.2257884.
18. Silva B, Moreira CL, Leite H, Peças Lopes JA. Control strategies for AC fault ride through in multiterminal HVDC grids. IEEE Trans Power Deliv. 2014;29(1):395–405. doi:10.1109/TPWRD.2013.2281331.
19. Zhou H, Yao W, Zhou M, Ai X, Wen J, Cheng S. Active energy control for enhancing AC fault ride-through capability of MMC-HVDC connected with offshore wind farms. IEEE Trans Power Syst. 2023;38(3):2705–18. doi:10.1109/TPWRS.2022.3179443.
20. Zhu Y, Li Y, Li B, Li T, Xu L, Liu N. Internal energy distribution control based fault ride-through and postfault recovery strategy for offshore wind farms connected to DR-MMC HVDC under onshore AC grid faults. IEEE Trans Sustain Energy. 2025;16(2):1191–205. doi:10.1109/TSTE.2024.3509963.
21. Ye H, Chen W, Yuan H, Zheng J. Analysis and protection of valve-side faults in offshore bipolar MMC-HVDC systems based on active neutral voltage shift. Int J Electr Power Energy Syst. 2025;172:111089. doi:10.1016/j.ijepes.2025.111089.
22. Qi L, Wu S, Zhang X, Zhang M, Liu C, Wang H, et al. A low-cost DC chopper with coupling transformer for offshore wind VSC-HVdc system. IEEE Trans Power Electron. 2022;37(5):4979–84. doi:10.1109/TPEL.2021.3135286.
23. Ndreko M, Rueda JL, Popov M, van der Meijden MAMM. Optimal fault ride through compliance of offshore wind power plants with VSC-HVDC connection by meta-heuristic based tuning. Electr Power Syst Res. 2017;145:99–111. doi:10.1016/j.epsr.2016.12.024.
24. Xiao F, Yin X, Tang J, He Q, Zhou K, Tang C, et al. A fault ride-through strategy for accurate energy optimization of offshore wind VSCHVDC system without improved fault ride-through strategy of wind turbines. Comput Electr Eng. 2024;118:109292. doi:10.1016/j.compeleceng.2024.109292.
25. Lee J, Yoo Y, Yoon M, Jang G. Advanced fault ride-through strategy by an MMC HVDC transmission for off-shore wind farm interconnection. Appl Sci. 2019;9(12):2522. doi:10.3390/app9122522.
26. Zhou H, Yao W, Sun K, Zong Q, Zhao H, Wen J. Enhancing fault ride-through and voltage support capability for MMC-HVDC integrated offshore wind farms based on multi-mode matching. IEEE Trans Sustain Energy. 2024;15(2):1256–68. doi:10.1109/TSTE.2023.3337782.
27. Mossa MA, Mahmoud H, Hassan AA, AL-Sumaiti AS. Dual-mode optimal predictive control of a wind driven multi-phase PMSG: a hybrid approach to grid and standalone applications. Results Eng. 2025;28:107105. doi:10.1016/j.rineng.2025.107105.
28. Liu P, Zhu G, Ding L, Gao X, Jia C, Ng C, et al. High-voltage ride-through strategy for wind turbine with fully-rated converter based on current operating range. Int J Electr Power Energy Syst. 2022;141:108101. doi:10.1016/j.ijepes.2022.108101.
29. GB/T 19963.2-2024. Technical specification for connecting wind power plant to power system-part 2: offshore wind power. Beijing, China: National Technical Committee for Standardization of Electric Power Supervision; 2024.
30. Yang Z, Gao B, Cao Z, Fang J. Grid-impedance-based transient current control for offshore wind turbines under low-voltage fault. J Mar Sci Eng. 2024;12(5):691. doi:10.3390/jmse12050691.